Engineered Science
DOI: https://dx.doi.org/10.30919/es975

Electrospinning with Natural Rubber and Ni Doping for Carbon Dioxide Adsorption and Supercapacitor Applications

Songwuit Chanthee,[1] Channarong Asavatesanupap,[2] Darunee Sertphon,[3] Thanigan Nakkhong,[4] Nakarin Subjalearndee[5] and Malee Santikunaporn[1,*]

Abstract

Three distinctive morphologies of carbon nanofibers (CNFs) on the surface were successfully fabricated by the electrospinning technique. The polymeric precursor was prepared by dissolving polyacrylonitrile (PAN), natural rubber (NR) cup lump, and nickel-pyridine complex in a single solution. The PAN-based polymeric solution, doped with various amounts of Ni, NR, and NR-Ni, was electrospun to create polymeric fibers and then stabilized and carbonized to obtain PAN composite nanofibers. Smooth surfaces were found on all NR-doped and Ni (5 wt%)-doped CNFs. Pores and spots on the CNFs' surface occurred on Ni-doped CNFs at 10 and 15 wt%, respectively. Interestingly, carbon nanotube (CNT) growth on the CNF surface was found in NR-10Ni@CNF samples. Depending on the preparation technique, Ni^0 nanoparticles also formed in CNFs, with a small size (25 nm) promoting CNT formation and a large size (200-400 nm) creating pores on the CNF surface. CNT growth on the carbon fiber surface was successfully achieved using trace amounts of NR with Ni samples. Based on the results of CO_2 adsorption and electrochemical performance, the 1NR-10Ni@CNF electrode exhibited a specific capacitance that was twice as high as the PAN electrode. Additionally, the 5Ni@CNF demonstrated CO_2 adsorption that was 4.0 times greater at 273 K and 2.9 times greater at 298 K.

Keywords: Carbon Nanofibers; Natural Rubber; Nickel Particles; CO_2 Adsorption; Supercapacitor.
Received: 16 August 2023; Revised: 29 September 2023; Accepted: 03 October 2023.
Article type: Research article.

1. Introduction

Carbon nanofibers (CNFs), a one-dimensional (1D) nanostructured carbon form, are drawing more and more interest as potential materials for a variety of applications due to their light weight, great physical strength, and chemical resistance[1]. Nanocomposites,[2] catalyst supports,[3] rechargeable batteries,[4] textiles,[5] supercapacitors,[6] energy devices,[7] and hydrogen storage.[8] are just a few of the potential uses for CNFs. Different CNF morphologies are needed for each application in order to improve its qualities. For instance, the CNF surface needs to have small pores and a large surface area for catalytic or hydrogen storage applications.[3,9] The size and surface area of CNFs determines their physical properties,[10,11] whereas tunable metal form and particle size inside the CNF matrix are required for superconductor applications. Controlling the size, surface area, and unique CNF morphology that match each application, however, is a difficult undertaking. There is growing interest in the use of CNFs supported by transition metal nanoparticles (Pd, Pt, Rh, Ru, Ir, Ni, etc.) as catalysts.[12] As an illustration, Ni/CNFs was employed as a catalyst for methane decomposition[13] and the hydrogenation reactions of benzene,[14] 2-tert-butylphenol,[15] and p-nitrophenol.[16] However, the decorated Ni was mostly achieved by

[1] *Department of Chemical Engineering, Faculty of Engineering, Thammasat School of Engineering, Thammasat University, Pathum Thani 12120, Thailand.*
[2] *Department of Mechanical Engineering, Faculty of Engineering, Thammasat School of Engineering, Thammasat University, Pathum Thani 12120, Thailand.*
[3] *Department of Chemistry, Faculty of Science, Rangsit University, Pathum Thani 12000, Thailand.*
[4] *Division of Materials and Textile Technology, Faculty of Science and Technology, Thammasat University, Pathumthani 12120, Thailand.*
[5] *National Nanotechnology Center, National Science and Technology Development Agency, 111 Innovation Cluster 2 (INC2 Building) Thailand Science Park, Pathum Thani 12120, Thailand.*
**Email:* smalee@engr.tu.ac.th (M. Santikunaporn)

conventional preparation methods such as impregnation, deposition-precipitation, and co-precipitation.

Polymeric electrospinning and conventional chemical vapor growth are two developed CNF fabrication techniques. Uniform CNFs are produced by chemical vapor growth, although this process is time-consuming and costly. On the other hand, electrospinning is a useful method for producing polymeric nanofibers. Additionally, the electrospinning technique offers chances to develop the architecture, functioning, chemical content, and shape of the fiber.[17] In addition, electrospinning is a widely recognized technique for producing functional nanofibers on an industrial scale due to its ease of use and versatility in processing various polymers.[18] To fabricate polymeric fibers prior to the carbonizing process, a variety of polymer sources are available, such as polyacrylonitrile (PAN),[19] polyvinyl alcohol (PVA),[20] polyvinylpyrrolidone (PVP),[21] pitch,[22] and rayon.[23] The best carbon yield is achieved by CNFs derived from the as-spun PAN precursor; nevertheless, PAN is a costly synthetic polymer.[24] Additionally, the benefit of as-spun PAN for human application demonstrates reduced genotoxicity in comparison to conventional CNFs.[25-27] As was previously said, many techniques have been used to synthesize carbon nanostructures in an effort to create a variety of surface morphologies. For instance, volatile organic solvents drive pore formation,[28] carbon additives improve surface area,[29] and mixed polymeric precursors promote branches on the surface of carbon nanofiber.[30] The use of green chemistry, which is environmentally beneficial and substitutes natural resources for dangerous compounds, is also growing in popularity.[31,32]

As a bioresource, natural rubber (NR) has been used as a filler in a variety of products, including carbon compounds, composites, and polymers.[33,34] The use of NR as an additive or precursor for electrospun polymeric fibers has not been documented. The NR structure's carbon chain may improve the texture of the carbon nanofiber by raising its carbon content, increasing defects, and causing the interior carbon fiber to become porous. In this study, metallic nickel doping was utilized to improve the unique surface morphologies of carbon nanotubes (CNTs), pores, and spots on CNFs. NR was employed as a co-precursor with PAN. Different behaviors of Ni particles in metallic form in CNFs were evaluated, as well as standard approaches to manage Ni particles as dopant in metallic form utilizing PAN-based carbon nanofiber under conventional heat treatment. The impact of three different concentrations of Ni (5, 10, and 15 wt%), and NR (0.5, 1.0, and 2.0 wt%) on the morphology and characteristics of fabricated CNFs was examined using three different sets of CNFs (Ni-PAN, NR/PAN, and Ni-NR/PAN). Thermogravimetric analysis (TGA), Fourier transform infrared spectroscopy (FTIR), Raman spectroscopy (RS), X-ray diffraction (XRD), field emission scanning electron microscopy (FESEM), transmission electron microscopy (TEM) and adsorption-desorption analyzer (BET analysis) were among the common characterization techniques that were used. Additionally, the synthesized CNFs' electrochemical performance and CO_2 adsorption were assessed.

2. Experimental section

2.1 Materials

In this research work, all chemicals were commercially available and used without further purification. Polyacrylonitrile (PAN) (ca. MW = 150,000), nickel (II) nitrate hexahydrate ($Ni(NO_3)_2 \cdot 6H_2O$), and pyridine (C_5H_5N) were purchased from Sigma-Aldrich. N, N-dimethylformamide (DMF) was purchased from Carlo-Erba Reagents. Hexane was obtained from Macron Fine Chemicals. Raw natural rubber (NR) cup lumps were harvested from an agricultural farm in Thailand. Nitrogen gas (99.999% UHP) was supplied by S.I. Technology Co., Ltd. (Thailand). Polyvinylidene fluoride (PVDF, 99.9%, Mw ~ 600,000) was purchased from Xiamen Tob New Energy Technology, China. Carbon black (CB, super P conductive, 99+ %) was purchased from Alfa Aesar.

2.2 Preparation of CNFs

2.2.1 Preparation of Ni doped CNFs

As illustrated in Fig. 1, polymeric electrospinning was used to fabricate CNFs doped with nickel nanoparticles (NiNPs), and then conventional heat treatment was applied. Initially, 8 wt% of PAN solution was prepared by fully dissolving PAN polymer in DMF under a magnetic stirrer for 12 hours at room temperature.[11,35] The resulting solution was then vigorously mixed at room temperature with pyridine ligand and metal nitrate in complex forms[36] until a homogeneous solution was achieved. The PAN-based solution was supplemented with metal complexes at 5, 10, and 15 wt%. Nickel (II) nitrate complexes with equivalent pyridine ligands were used to generate a number of solutions with different metal complexes (5Ni-PAN, 10Ni-PAN, and 15Ni-PAN). A stainless steel gauge needle with an inner diameter of 1 mm was used to electrospun the polymeric solution precursors containing the produced metal complexes into polymeric fibers. The gauge needle was connected to the anode of a DC power source at a high voltage of 15 kV and a flow rate of 1 ml/h. A collector made of stainless steel roller was covered with a piece of aluminum foil.

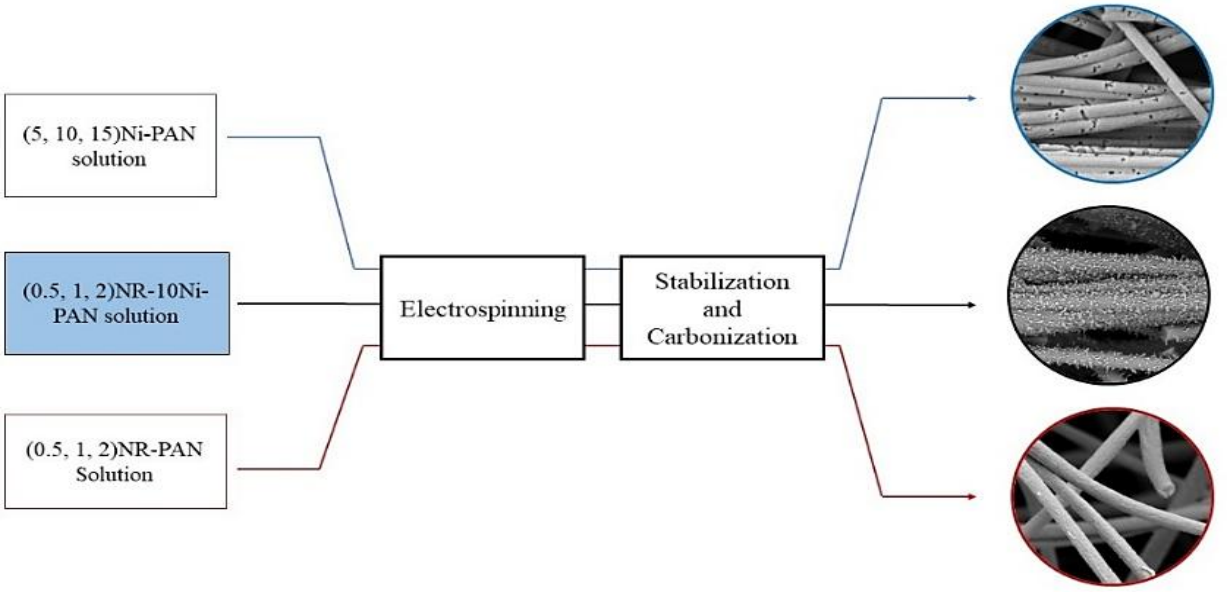

Fig. 1 Schematic illustration of the preparation process of nNi@CNF, nNR@CNF, and nNR-10Ni@CNF.

The process was carried out at room temperature. The needle tip and the collector were 15 cm apart. Finally, the thermal treatment was used to transform the as-spun fibers into carbon nanofibers. To develop NiNP-doped CNFs (denoted as 5Ni@CNF, 10Ni@CNF, and 15Ni@CNF), all as-spun fibers were stabilized at 533 K for 2 hours at a heating rate of 1 K/min. They were subsequently annealed at 1173 K with a heating rate of 10 K/min in an N_2 environment.

2.2.2 Preparation of NR doped CNFs

The NR-doped CNFs were fabricated in a procedure similar to the earlier preparation, which involved dissolving 8 wt% of PAN polymer in DMF for 12 hours at room temperature using a magnetic stirrer. Next, dried NR was thoroughly dissolved in hexane while being vigorously stirred for 12 hours at room temperature to form an NR solution. After an hour of vigorous stirring, the produced NR solution was gradually added to the 8 wt% PAN solution. In order to formulate the mixed polymeric solution, 0.5, 1, and 2 wt% (denoted as 0.5NR-PAN, 1NR-PAN, and 2NR-PAN) of NR were added to the PAN-based solution. Subsequently, a stainless steel gauge needle with an inner diameter of 1 mm was used to electrospun the mixed polymeric solution precursors into fibers. The gauge needle was coupled to a DC power source at a high voltage of 20 kV and a flow rate of 2 ml/h. A collector made of stainless steel rollers was covered with a piece of aluminum foil. The procedure was done at 303 K. The needle tip and the collector were separated by 15 cm. Ultimately, the resulting fibers underwent heat treatment at the same temperatures, durations, and heating rates mentioned in Section 2.2.1 to transform into carbon fibers. The obtained NR-doped CNFs were designated as 0.5NR@CNF, 1NR@CNF, and 2NR@CNF.

2.2.3 Preparation of NR and Ni doped CNFs

By combining the nickel (II) complex with the NR-PAN polymer, NR- and Ni-doped CNFs were prepared. The procedure described in Section 2.2.2 was used to prepare the 0.5, 1, and 2NR-PAN solutions. Next, three NR-PAN solution precursors were mixed with 10 wt% of nickel (II) nitrate and four equivalents of pyridine ligand to form the NR-PAN and Ni complex polymeric precursors (denoted as 0.5NR-10Ni-PAN, 1NR-10Ni-PAN, and 2NR-10Ni-PAN). The solution precursors were loaded into the syringe and placed in the electrospinning machine after being thoroughly mixed at room temperature for half an hour following the addition of all the components. The same parameters and conditions as described in Section 2.2.1 were applied when electrospunting the combined precursors into fibers. Finally, using the previously described procedure, heat treatment was used to transform the produced NR- and Ni-doped fibers into carbon. 0.5NR-10Ni@CNF, 1NR-10Ni@CNF, and 2NR-10Ni@CNF were the names of these CNFs.

2.3 Characterization

The chemical functional groups of the as-spun fibers were analyzed by Fourier transform infrared spectroscopy (FTIR) using a Spectrum 100 (PerkinElmer, USA). Data were collected using an attenuated total reflection (ATR) technique connected to infrared spectroscopy with 16 scans/sample. Thermal stability and weight loss of the as-spun fiber samples were determined by thermogravimetric analysis (TGA), a model TGA2 STARe system (Mettler Toledo, USA)

performed in the range of 313 to 973 K with a heating rate of 10 K/min under a nitrogen flow of 5 ml/min. The crystal structures of the samples were measured by Raman spectroscopy (RS) (HORIBA model KH 8700, Japan). Chemical components of all carbon fibers were recorded by powder X-ray diffraction (XRD) using a model D8 advanced X-ray diffractometer (Bruker, USA) equipped with a Cu Kα sealed tube X-ray source (1.5418 Å). Data were collected in the range of 5.0 to 60.0° for 2θ in steps of 0.02° with a scan speed of 0.1 sec/step. The average size of metal particles was estimated from the XRD data by the Scherrer equation, as presented in Equation (1).[37]

$$D = K \lambda / \beta \cos \theta \quad (1)$$

where D is the average particle grain size, K is a dimensionless factor (typical value = 0.9), λ is the X-ray wavelength, β is the line broadening at maximum intensity of full width at half maximum (WFHM), and θ is the Bragg angle. The physical morphology of the carbon fiber samples was detected by a field emission scanning electron microscope (FESEM), model Merlin Compact (Zeiss, Germany). Images were captured under an in-lens duo detector (in-lens secondary electron (SE) and energy selective backscattered detection (EsB)) and a transmission electron microscope (TEM), model Tecnai G2 20 S-Twin (FEI, USA) at an operating voltage of 200 kV. The gas adsorption-desorption experiment (up to 1 bar) was performed on a Quantachrome Autosorb automated gas sorption analyzer.

2.4 Supercapacitor device assembly and electrochemical performance evaluation

Supercapacitor cells were assembled in two-electrode Swagelok cells using the PAN composite nanofibers (Ni-doped CNFs, NR-doped CNFs, and NR-Ni-doped CNFs) as a major component in the electrodes, 2 M sulfuric acid as the electrolyte, and filter paper (Whatman filter paper No. 4) as the membrane separator. The electrode was prepared by casting a slurry containing the PAN composite nanofibers, carbon black, and PVDF binder in a weight ratio of 7:2:1, respectively, on stainless-steel foil before drying inside a vacuum oven at 353 K overnight. The dried electrode was then punched into a circular sheet with a diameter of 80 mm before being assembled in the Swagelok cells. All electrochemical characterizations were measured at room temperature. Cyclic voltammetry (CV) and galvanostatic charge-discharge (GCD) were conducted by an electrochemical workstation (Metrohm Autolab, PGSTAT302N). The specific capacitance of the PAN composite nanofiber electrodes was evaluated from GCD curves according to Equation (2).[38]

$$CSC = 4I\Delta t / m\Delta V \quad (2)$$

where CSC is a specific capacitance (F/g), I is a constant discharge current (A), Δt is a discharge time, m is the electrode mass (g), and ΔV is a potential change (V).

2.5 CO_2 adsorption measurements

CO_2 adsorption isotherms were measured on an Autosorb iQ-MP/XR (Quantachrome) at 273 and 298 K. 80 mg of sample in a sample cell were degassed at 553 K for 18 hours under a He environment before the measurement. The adsorption isotherms were recorded at pressures ranging from 0-100 kPa while flowing pure CO_2 (99.999 %).

3. Results and discussion

3.1 Characterization of synthesized carbon nanofibers

TGA was performed to investigate the optimal temperature and prevent polymeric decomposition in order to stabilize the as-spun fibers. Thermograms of a selection of as-spun fibers are shown in Fig. 2. Due to the decomposition of compounds containing oxygen, nitrogen, and hydrogen during the carbonization process,[39] the 1NR-PAN demonstrated a single step of significant weight loss of 29% at 310 °C (583 K) in the carbonization process. On the other hand, three steps of weight loss were shown by the TGA curves of 10Ni and 1NR-10Ni-PAN. First, weight loss occurred between 50 °C (323 K) and 110 °C (383 K), corresponding to when the humidity was removed; second, weight loss occurred between 175 °C (448 K) and 260 °C (533 K), which is when the pyridine ligand dissociated. At 300 °C (573 K), the final stage represented carbonization and decomposition. Consequently, 260 °C (533 K) was chosen as the stabilization temperature.

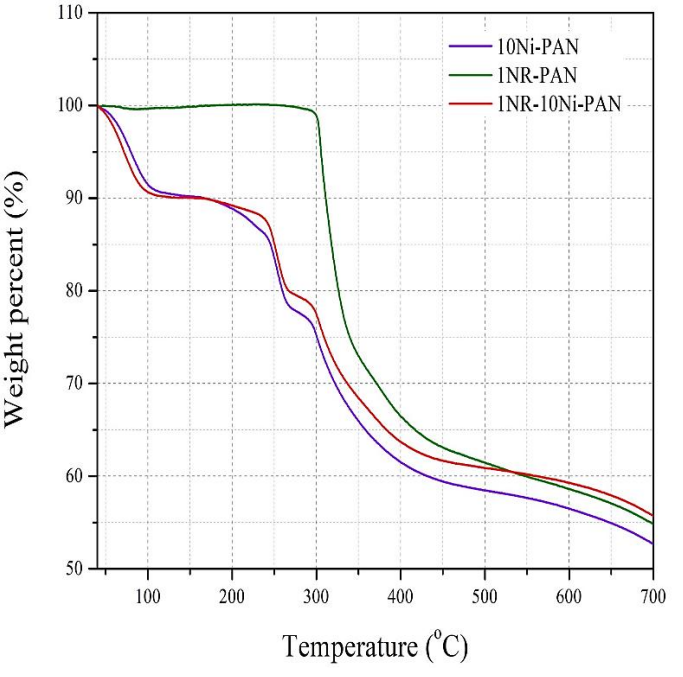

Fig. 2 TGA curves of 10Ni-PAN (green), 1NR-PAN (brown), and 1NR-10Ni-PAN (blue) as-spun fiber.

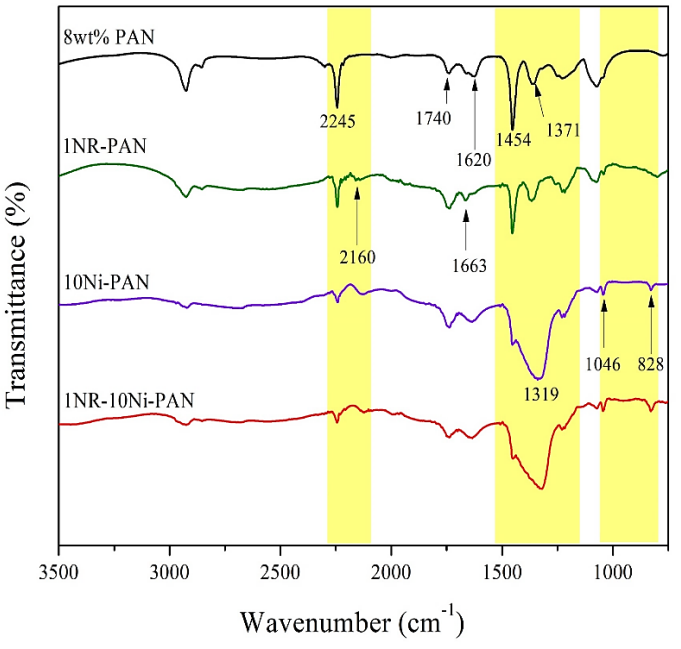

Fig. 3 FTIR spectra of as-spun fibers.

The 8 wt% PAN, 1NR-PAN, 10Ni-PAN, and 1NR-10Ni-PAN as-spun fibers were selected to characterize the chemical functions by FTIR, as shown in Fig. 3. The vibrational frequencies of the as-spun nanofibers were presented in the range of 3500 to 750 cm^{-1}. Different dopant fibers showed clear characteristic signals, in agreement with the 8 wt% PAN spectrum at 2923, 2245, and 1454 cm^{-1} of C−H stretching, C≡N group, and C−H bending, respectively.[40] The spectrum of 1NR-PAN presented the characteristic vibration of PAN and showed a weak absorption band at 2160 cm^{-1} assigned to C=C stretching and a weak band at 1663 cm^{-1} assigned to substituted C=C stretching.[41] The C=C vibrations in the 1NR-PAN spectrum implied that NR had dispersed in PAN fibers. For 10Ni-PAN and 1NR-10Ni-PAN spectra, the vibrational frequencies revealed similar patterns resulting from Ni-pyridine complex addition and the poor signal of NR. The distinct weak broad bands around 2160 and 1663 cm^{-1} were assigned to C=C stretching, while the strong broad vibration at 1319 cm^{-1} corresponded to the C−N group of disordered pyridine ligands in the Ni-pyridine complex.[42] Moreover, characteristic aromatic peaks at 1046 and 828 cm^{-1} were attributed to the pyridine ring structure, while the absorption band at 1740 cm^{-1} was assigned to C=O stretching of the residue solvent (DMF). In the 1NR-10Ni-PAN spectrum, the Ni metal signal could not be seen. However, the vibration of the coordinated pyridine ligand was used to show that the metal complex had been added. The wavenumber of free pyridine ligand (1433 cm^{-1}) shifted to a lower value when coordinated to the metal core,[43] while broad frequencies between 1400 and 1322 cm^{-1} were assigned to coordinated pyridine ligand due to the lower shift and wide wavenumber frequency range.

All the fabricated CNF samples were characterized by Raman spectroscopy. In Fig. 4, the D-band (blue region) at 1355 cm^{-1} reflected disordered graphite in CNF, while the G-band (yellow region) around 1580 cm^{-1} was caused by ordered graphite or carbon fibers with sp^2 hybridization.[44] The presence of the D-band implied that the CNFs had defects due to impurities, incomplete graphitization, and sp^3 hybridization. An increase in the ratio of D- to G-band intensity revealed the level of defects and impurities in the CNF structure, with a higher ratio indicating lower crystallizability of the carbon fibers. The D-band/G-band ratio for nNR@CNF samples rose with increasing NR content because the NR dopants were not carbon-based for graphitization. As a result, when adding larger amounts of NR, a slightly growing value of D-band/G-band ratio influences the samples' reduced crystallizability. Of the Ni-doped CNFs, 10Ni@CNF had the greatest D-/G-band intensity ratio (I_D/I_G =1.03), followed by 5Ni@CNF with a moderate ratio (0.97) and 15Ni@CNF with the lowest ratio (0.79). Ni particles incorporated in the CNF structure caused this variation. Remarkably, compared to pure NR- and Ni-doped CNF, the ratios of NR and Ni CNF (nNR-10Ni@CNF samples) were lower. As previously mentioned, NR- and Ni-doped CNFs demonstrated decreased crystallizability while increasing sp^2 carbon formation and improving graphitization. X-ray diffraction patterns from carbon nanofibers that were produced are shown in Fig. 5. The disordered structure of the carbon phase was confirmed by the large diffraction peaks between 25 and 35 degrees of 2θ.[15] According to earlier findings,[45] the diffraction pattern of synthesized 8 wt%-PAN@CNF revealed the carbon phase pattern of carbon nanofibers. The small peak at 2θ = 26 degrees of the 10Ni@CNF and 15Ni@CNF patterns for Ni doped carbon nanofibers was attributed to the reflection (002) of carbon because of a more graphitic structure of the carbon fibers or carbon bonded to Ni.[46] While 5Ni@CNF had diffraction peaks at 2θ = 37 (111) and 43 (200) degrees of NiO,[46] all Ni-doped CNFs showed sharp diffraction peaks at 2θ = 44 (111) and 52 (200) degrees as typical peaks of metallic Ni. It is interesting to note that only Ni (0) peaks were seen in the XRD patterns of 10Ni@CNF and 15Ni@CNF because the pyridine ligand arranged around the Ni metal core inhibited Ni oxidation during the heating process. Nonetheless, incomplete complexation for low concentrated Ni and pyridine in the polymeric solution led to the observation of NiO particles in 5Ni@CNF. 10Ni@CNF was chosen to dope with trace NR because it had the lowest Ni content in metallic form. As expected, different concentrations of NR dopant with 10 wt%

Ni carbon nanofibers exhibited the Ni^0 pattern and no NiO formation.

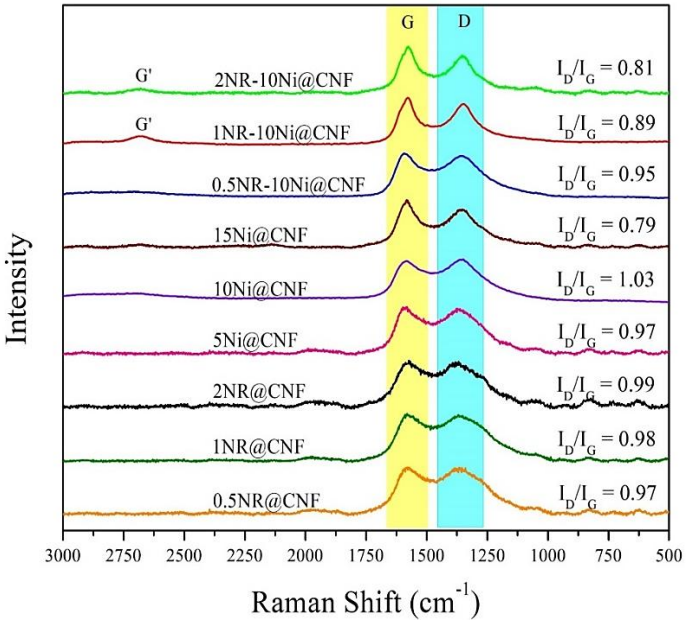

Fig. 4 Raman spectra of carbon nanofibers.

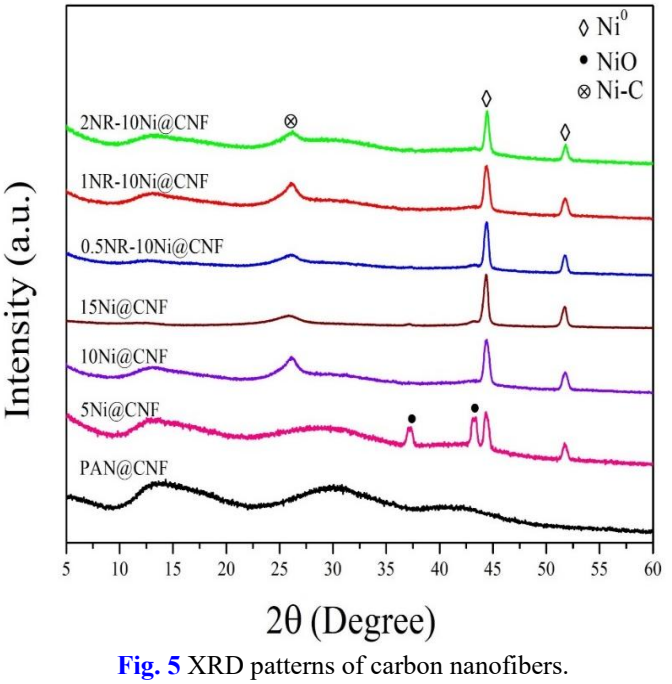

Fig. 5 XRD patterns of carbon nanofibers.

Average sizes of metal particles were estimated from the XRD data by the Scherrer equation.[37] as presented in Table S1. By using a common value of K = 0.9, the Ni^0 particle size was calculated to be between 15 and 18 nm, and the calculated NiO particle size in 5Ni@CNF was 15.04 nm. The computed Ni particle size demonstrated good particle dispersion and demonstrated that this approach could detect doped Ni particles on a nanometric scale. Particle sizes were found to be dispersed between 25 and 30 nm for small sizes and between 130 and 250 nm for large sizes, in contrast to the TEM approach as illustrated in Fig. 6. Some large Ni particles aggregated during polymeric solution or graphitization processes.

Based upon the results herein and the precedent reports, a plausible reaction pathway is shown in Fig. 7. At the polymeric solution preparation step, the nickel nitrate ($Ni(NO_3)_2$) was surrounded by excess pyridine ligands, which led to the formation of the square planar $[Ni(py)_4(NO_3)_2]$ complex.[47,48] However, when excess pyridine was added to the solution precursor, other forms of Ni complexes were created with 2, 3, or 6 pyridine compounds in the solution, such as $[Ni(py)_2(NO_3)_2]$, $[Ni(py)_3(NO_3)_2]$, and $[Ni(py)_6(NO_3)_2]$.[49,50] Subsequently, the Ni (II) complex changed to NiNPs by removing pyridine compounds at high temperatures in the stabilization and carbonization steps. In these steps, the pyridine compound that surrounded the Ni^{2+} ion probably prevented the oxidation of Ni to nickel oxide.

The morphologies of carbon nanofibers with different dopants were determined by SEM and TEM. As shown in Figs. 8(a-c), SEM images of various Ni-doped CNFs had different morphologies as smooth surfaces with pores and spots for 5Ni@CNF, 10Ni@CNF, and 15Ni@CNF, respectively. With well-dispersed Ni^0 nanoparticles (25 nm) and a small diameter (250-350 nm), the 5Ni@CNF possessed a smooth and uniform surface. The XRD result led to the assignment of Ni^0 (25 nm) and NiO (200 nm) forms to the two sizes of Ni particles. In comparison, the diameter of 10Ni@CNF was bigger (average 633 nm) and it had a porous surface. Ni agglomerated into larger particles when the amount of Ni dopant was increased to 10 wt%, even though Ni-doped CNF was only found in Ni^0 form. These Ni^0 particles (250 nm) were larger than Ni particles in 5Ni@CNF. Additionally, Ni nanoparticle drilling had an impact on pores that were present throughout the carbon fiber chain.[51] As shown in Fig. 6(b), the Ni particles destroyed the carbon matrix adjacent to their surface by creating pores on the surface.[52-54] According to the TEM images, there is evidence that Ni^0 particles punched holes in the CNF matrix, causing pore development on CNFs. NiNPs were found at the bottom of these pores. The 10Ni@CNF sample and 15Ni@CNF particles exhibited comparable diameters (average 849 nm). Large spots of Ni particles were detected all over the CNF surface, however pores were not visible on the surface of 15Ni@CNF. The higher Ni concentration in CNF promoted the production of NiO under thermal conditions and aided in the agglomeration of the bigger particles.[55]

The surfaces of the three NR-doped CNF samples were all smooth. The average diameters of NR-doped CNF for 0.5NR@CNF, 1NR@CNF, and 2NR@CNF were 422, 433,

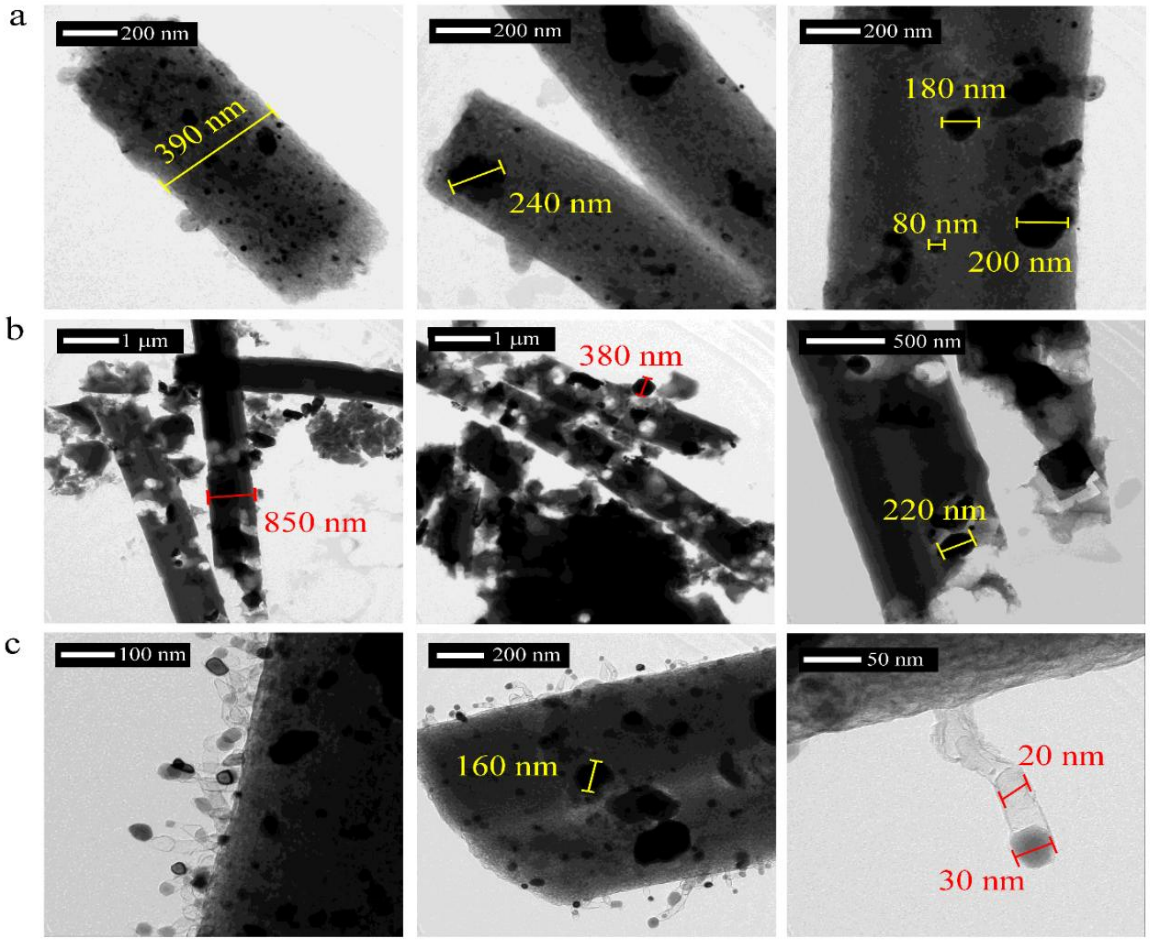

Fig. 6 TEM images of (a) 5Ni@CNF, (b) 10Ni@CNF and (c) 0.5NR-10Ni@CNF.

and 676 nm, respectively, as shown in Figs. 9(a-c). The greater concentration of NR doped in solution during the electrospinning polymeric fiber process led to an increased in diameter. The diameter size was affected, and the electrospinning process was impeded by the increased NR dopant level. Furthermore, the NR dopant both interrupted the graphitization process and increased the diameter size, as reported in the Raman characterization. This suggests that NR can be employed as a carbon source or additive for CNF fabrication. However, due to incompatibility between PAN precursor and NR during the preparation of polymeric precursor, NR doping over 2 wt% could not be electrospun into fibers.

Interestingly, as shown in Figs. 10(a-c), branches of carbon nanotube growth over their mother CNF were visible in the three SEM images when NR was varied from 0.5, 1, and 2 wt% to Ni (10 wt%) CNF. For 0.5NR-10Ni@CNF, 1NR-10Ni@CNF, and 2NR-10Ni@CNF, the average CNF size was 789.63, 879.52, and 1,890.54 nm, respectively. Ni nanoparticles catalyzed the growth of the carbon nanotubes that were detected on the CNF surface.[56] The agglomerated Ni particles in 10Ni@CNF with NR doping disintegrated into the carbon matrix surrounding the Ni particles, whereas the

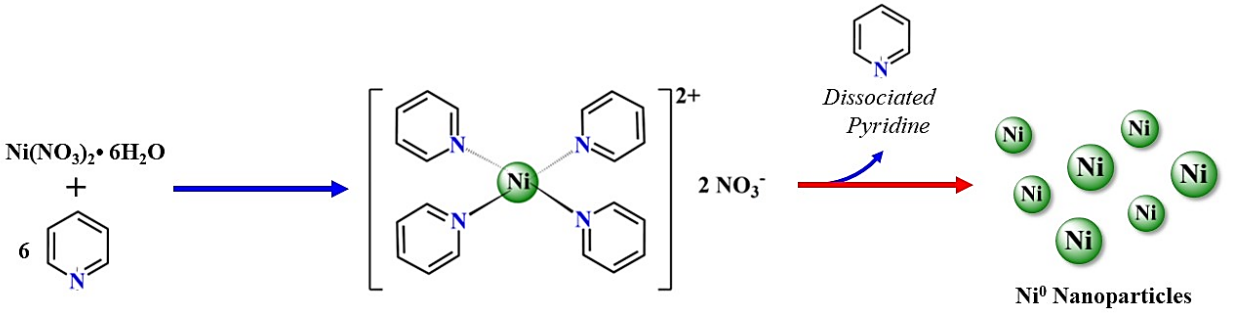

Fig. 7 Proposed mechanism for NiNPs formation after coordinated by pyridine ligand.

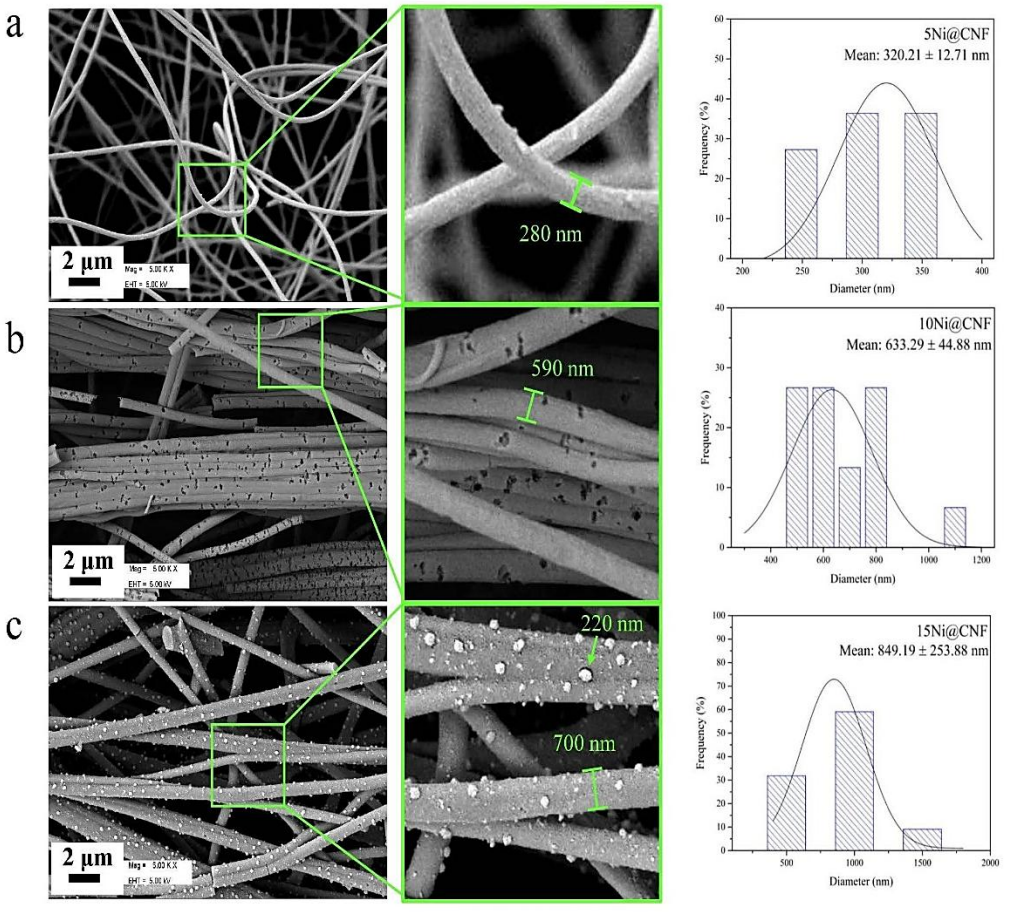

Fig. 8 SEM images (left) and diameter size distribution (right) of (a) 5Ni@CNF, (b) 10Ni@CNF, and (c) 15Ni@CNF samples.

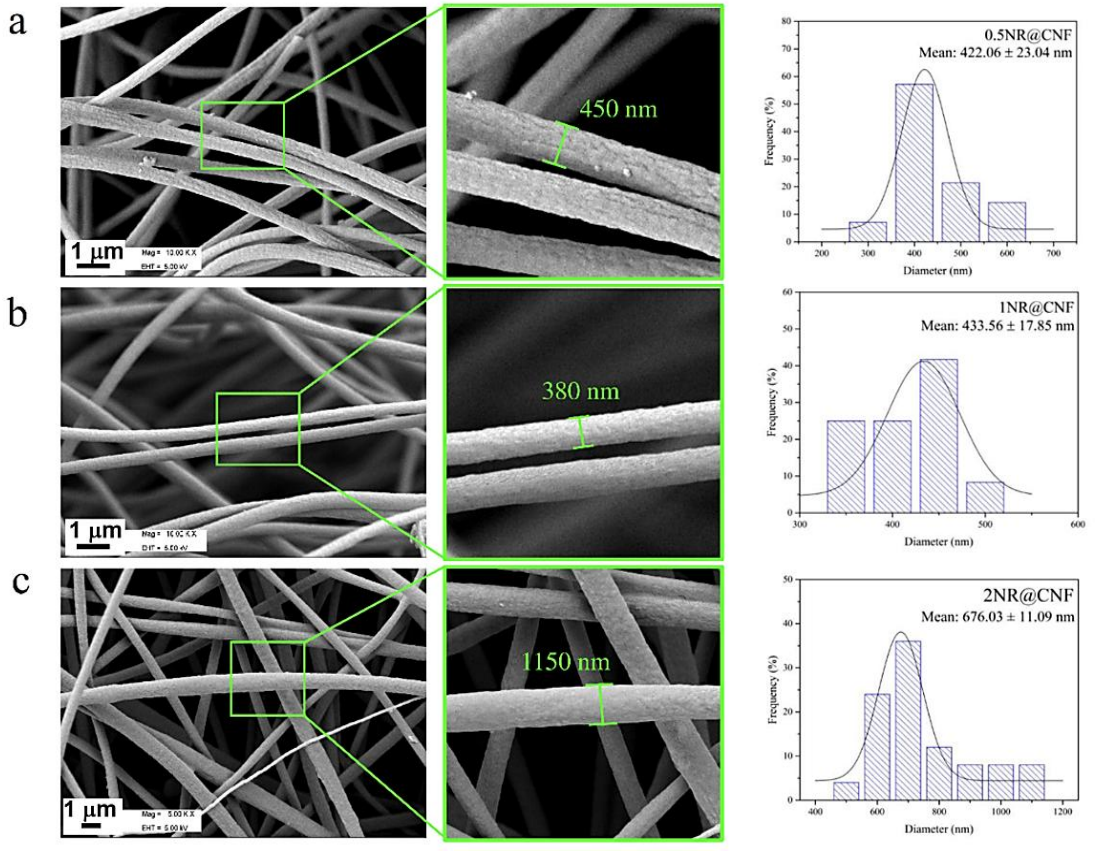

Fig. 9 SEM images (left) and diameter size distribution (right) of (a) 0.5NR@CNF, (b) 1NR@CNF and (c) 2NR@CNF samples.

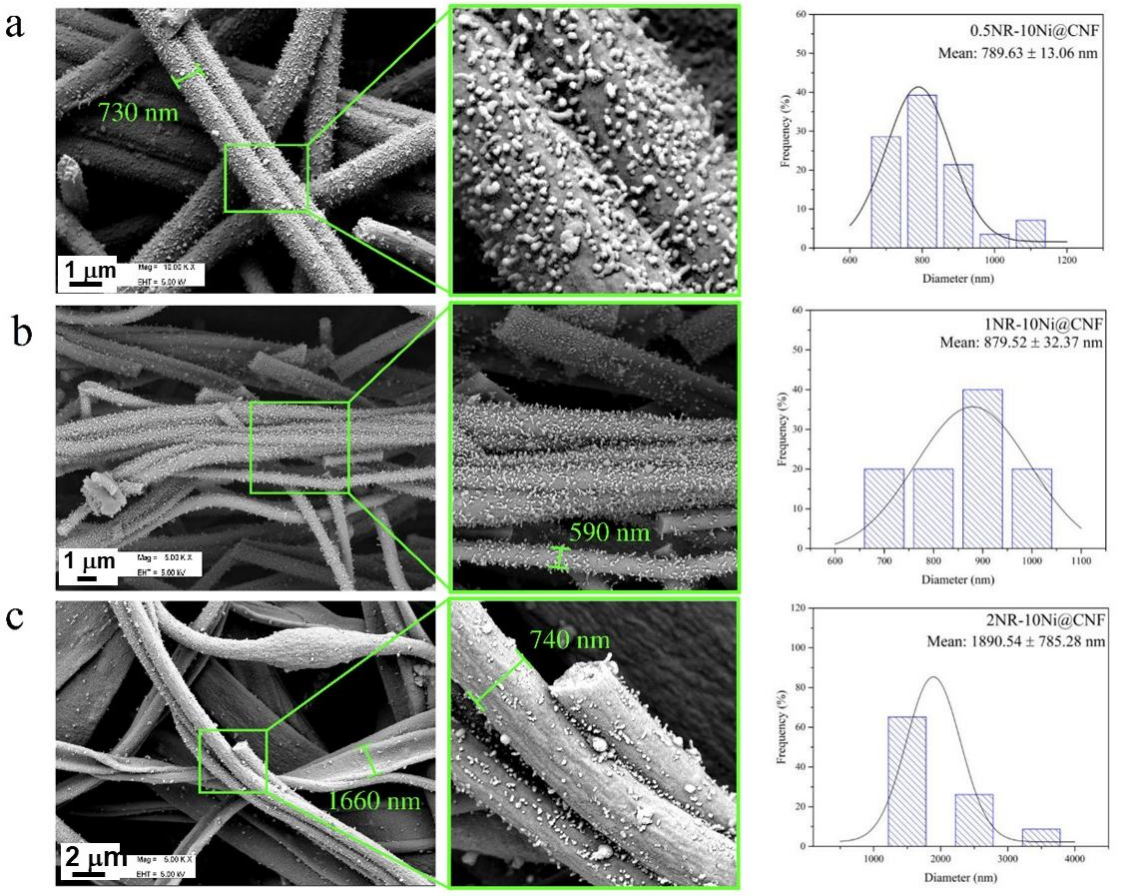

Fig. 10 SEM images (left) and diameter size distribution (right) of (a) 0.5NR-10Ni@CNF, (b) 1NR-10Ni@CNF and (c) 2NR-10Ni@CNF samples.

smaller Ni particles (27 nm) in 10Ni@CNF with NR doping promoted accelerated carbon nanotube growth. Because of the poor non-graphitized carbon in the carbon fiber, the Ni particles of 5Ni@CNF did not promote the formation of carbon nanotubes. Since the chemical nature of NR allows carbon decomposition to become a carbon resource, Ni particles of NR-doped CNF in 10Ni@CNF can act as a catalyst for carbon nanotube growth. The 0.5NR-10Ni@CNF was characterized by TEM in order to verify that Ni nanoparticles stimulated the growth of carbon nanotubes, as demonstrated in Fig. 6(c), and they distinctly protruded from their mother surface.

The CNF growth process with ethylene decomposition on Ni and Ni/C catalysts was proposed by Prasiwi et. al.[51] Similarly, NR was decomposed at high temperatures during the carbonization step, and Ni nanoparticles on the surface of CNF searved as the active nucleation sites for the formation of CNTs. Furthermore, these carbon nanotubes' diameter was in agreement with other reports[56,57] because it was near the Ni size. Because the higher non-compatible NR concentration led to poor NR dispersion in the PAN polymer and as-spun fiber form, the 2NR-10Ni@CNF had the biggest diameter of CNF and the lowest growth of carbon nanotubes.

To quantify the surface area of the materials, nitrogen adsorption-desorption studies of all samples were carried out using the BET method; the results are shown in Table 1. An adsorption-desorption of 5Ni@CNF, 10Ni@CN, and 15Ni@CNF is presented in Fig. 11(a). The 5Ni@CNF showed a type I isotherm with a surface area of 396.72 m^2 g^{-1}, which was associated with its smallest size. On the other hand, the 10Ni@CNF and 15Ni@CNF samples were classified as type IV isotherms, which are typical of mesoporous solids that go through monolayer and multilayer hysteresis, then capillary condensation during desorption.[58,59] In contrast to the 10Ni@CNF sample, which had pores on its surface and the lowest surface area (66.23 m^2g^{-1}) due to CNF bunch formation, the 15Ni@CNF sample had a moderate surface area (144.07 m^2g^{-1}) and less CNF bunches. Depending on the concentration of Ni doping, the specific surface area of the nNi@CNF samples varied from 60 and 400 m^2 g^{-1}.

Nitrogen adsorption-desorption isotherms of type I for 0.5NR@CNF, 1NR@CNF, and 2NR@CNF are shown in Fig. 11(b), suggesting a consistent CNF surface for all NR doped samples. In accordance with the bigger diameter of

Table 1. Physicochemical properties of Ni doped carbon nanofiber.

Sample	BET surface area (m^2/g)	Pore volume (cm^3/g)	Pore width (nm)
5Ni@CNF	396.27	0.0312	2.02
10Ni@CNF	66.23	0.0326	3.45
15Ni@CNF	144.07	0.0562	2.77
0.5NR@CNF	26.32	0.0076	2.88
1NR@CNF	14.60	0.0104	5.28
2NR@CNF	5.77	0.0102	6.60
0.5NR-10Ni@CNF	169.99	0.0850	3.13
1NR-10Ni@CNF	79.38	0.0613	4.07
2NR-10Ni@CNF	62.91	0.1019	6.53

greater NR-doped CNF, specific surface areas of 0.5NR@CNF, 1NR@CNF, and 2NR@CNF were 26.23, 14.60, and 5.77 m^2 g^{-1}, respectively, and decreased with an increase in NR polymer quantity. Furthermore, in accordance with previous studies,[60] 1NR@CNF and 2NR@CNF isotherms showed poor N_2 adsorption on carbon-based materials. The nitrogen adsorption-desorption isotherms for 0.5NR-10Ni@CNF, 1NR-10Ni@CNF, and 2NR-10Ni@CNF are shown in Fig. 11(c). 0.5NR-10Ni@CNF, 1NR-10Ni@CNF, and 2NR-10Ni@CNF had specific surface areas of 196.99, 97.38, and 62.91 m^2 g^{-1} respectively. These areas dropped as NR polymer loading increased, leading to larger CNF diameters, which in turn caused a decrease in CNT formation on the mother carbon surface. Type IV isotherms for all samples showed small cylindrical pores on CNF surface branches.[58,59]

3.2 Electrochemical performance of PAN and PAN composite nanofiber electrodes

Among PAN composite nanofibers, NR-Ni-PAN composite nanofibers (NR-Ni@CNF) were chosen to evaluate their electrochemical performance as electrodes in supercapacitor cells due to their specific surface and mechanical characteristics. Prior to measuring the specific capacitance of PAN and NR-Ni-PAN composite nanofibers using GCD, their performances were assessed by CV at a scan rate of 50 mV/s within a range of 0-1.2 V. Overall, the voltammogram of the PAN nanofiber electrode showed similarity to a quasi-rectangular shape (Fig. 12(a)), whereas the PAN composite nanofiber electrode presented pseudocapacitive

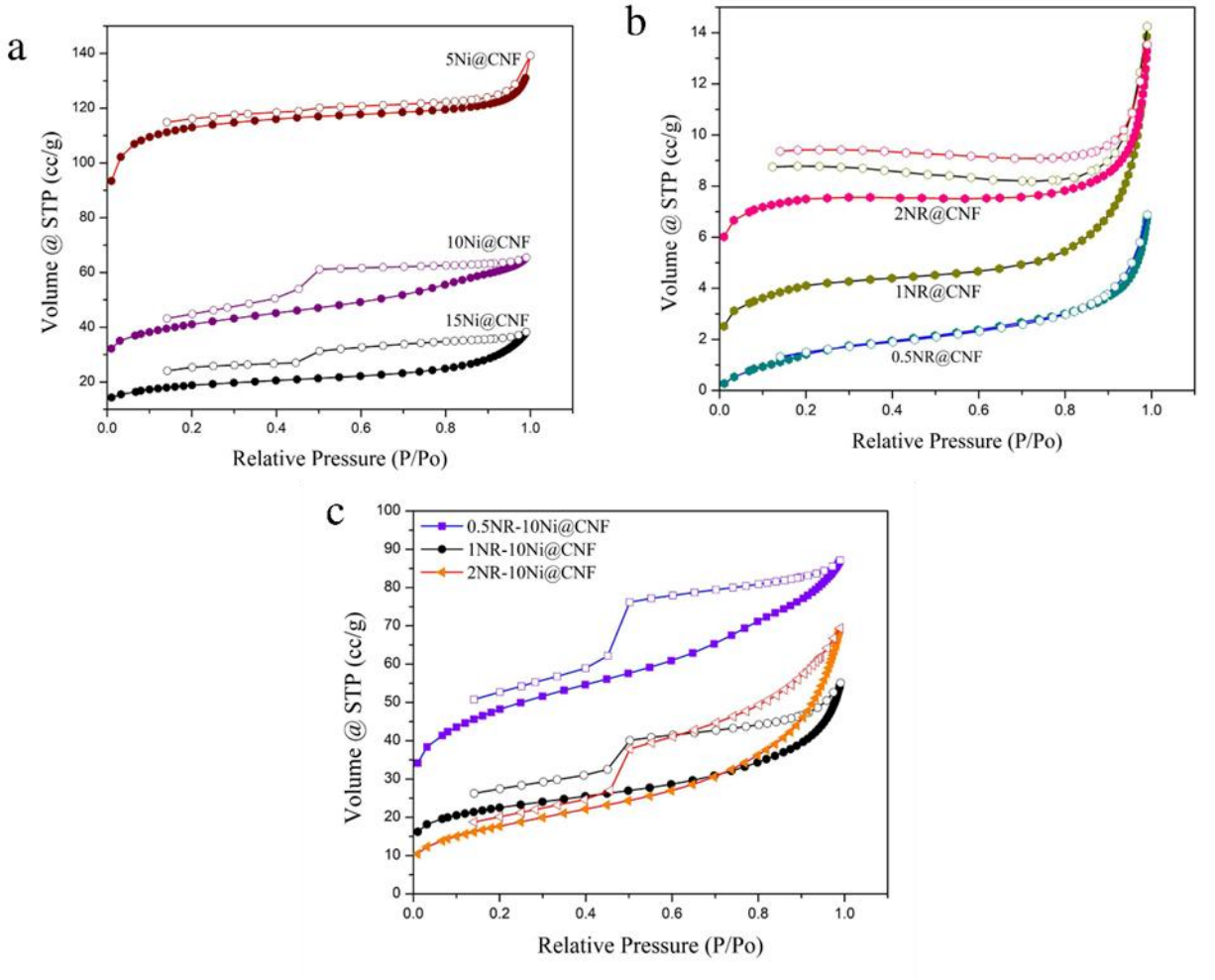

Fig. 11 The N_2 adsorption-desorption isotherms of (a) nNi@CNF, (b) nNR@CNF and (c) nNR-10Ni@CNF samples.

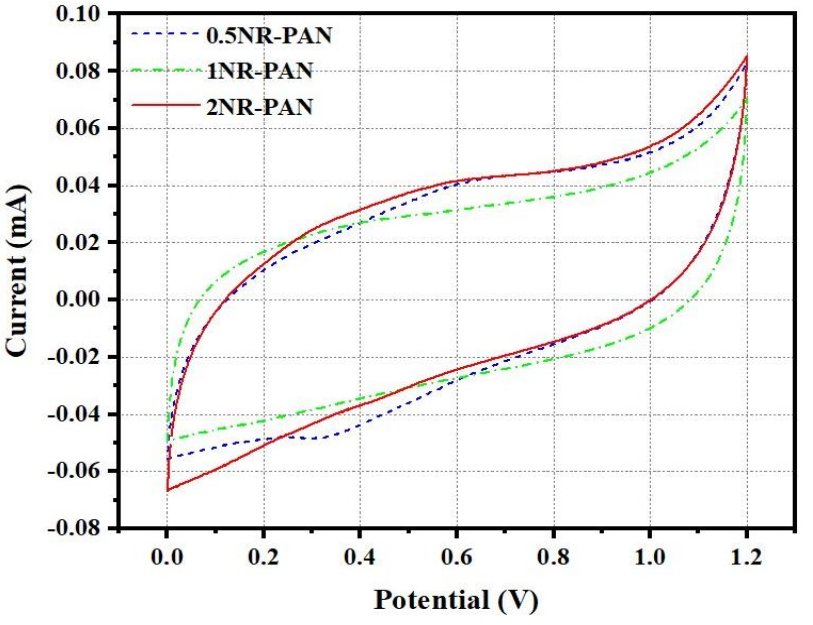

Fig. 12 Electrochemical performance of PAN and PAN composite electrodes. Cyclic voltammograms at scan rates of 50 mV/s of (a) PAN@CNF, (b) 0.5NR-10Ni@CNF, (c) 1NR-10Ni@CNF, and (d) 2NR-10Ni@CNF.

characteristics.[61] Small redox peaks were seen at around 0.52 and 0.67 V in the PAN composite electrode with the lowest NR content, 0.5NR-10Ni@CNF (Fig. 12(b)). Greater voltammogram areas with redox peaks were obtained by increasing the NR content in the PAN composite nanofibers to 1 and 2 wt% (Figs. 12(c) and 12(d)). A litter redox peak was observed at around 0.52 V for the 1NR-10Ni@CNF electrode and between 0.58 and 0.85 V for the 2NR-10Ni-PAN electrode.[62] It was hypothesized that Ni nanoparticles promoted ion conduction,[63,64] while NR increased the porosity of the electrode.

Figure 13 presents the specific capacitance of PAN and PAN composite electrodes evaluated at a current density of 0.1 A/g and calculated using Equation (2). Overall, there was a good correlation between CV performance and specific capacitance. The average specific capacitance of the PAN electrode was approximately 40 F/g, whereas the average specific capacitances of the 0.5NR-10Ni@CNF, 1NR-

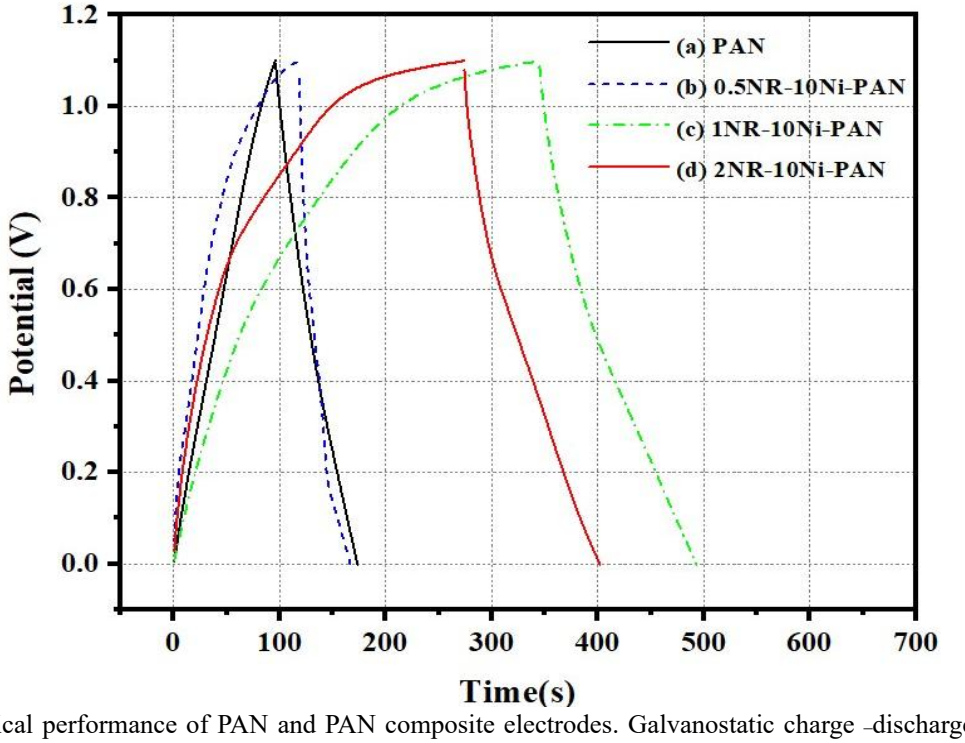

Fig. 13 Electrochemical performance of PAN and PAN composite electrodes. Galvanostatic charge–discharge profiles at current density of 0.1 A of (a) PAN@CNF, (b) 0.5NR-10Ni@CNF, (c) 1NR-10Ni@CNF, and (d) 2NR-10Ni@CNF.

10Ni@CNF, and 2NR-10Ni@CNF electrodes were approximately 25, 84, and 61 F/g, respectively. Among the PAN composite electrodes, the 1NR-10Ni@CNF showed a specific capacitance that was twice as high as the PAN electrode. The increased specific capacitance could be related to the pore characteristics of the PAN composite nanofibers.[65,66] Even though the charge-discharge performance was not as high as the previously published results,[67,68] it could be seen that incorporating NR and Ni nanoparticles into the PAN nanofiber electrode significantly improved the electrochemical performance. In addition, the physical characteristics of the PAN composite electrode after measuring the electrochemical performance were checked. Non-homogeneity of electrode between the PAN composite nanofibers and conductive carbon was found (Fig. S1). To improve the electrochemical performance of the PAN composite electrodes, optimization of electrode preparation processes was required.

3.3 CO_2 adsorption isotherms

According to Fig. 14, the CO_2 adsorption capacities of nNi@CNF samples are as follows: 5Ni@CNF > PAN@CNF > 15Ni@CNF > 10Ni@CNF. With a sharp rise at low relative pressure, the CO_2 adsorption isotherm of 5Ni@CNF shows the maximum CO_2 uptake at 273 K (137.95 cc/g) and 298 K (95.94 cc/g). This value is significantly greater than that of PAN@CNF at 273 K (33.91 cc/g) and 298 K (32.80 cc/g). Additionally, the CO_2 adsorption quantities on 5Ni@CNF were better than those on commercial activated carbon fibers (1.92 mmol/g)[69] at 273 K and 298 K, respectively, at 6.15 and 4.28 mmol/g. Although the smooth surfaces of these samples are identical, 5Ni@CNF showed a significant capacity to absorb CO_2 due to potential interactions between the NiNPs and CO_2 molecules. In contrast to earlier findings, 5Ni@CNF had the maximum CO_2 adsorption capacity at both temperatures. Additionally, those CNF samples had a hollow cylindrical shape, a high surface area, and high porosity.[70-74] Table 2 lists the CO_2 adsorption capacity for various dopants and CNF morphologies. This 5Ni@CNF exhibits moderate S_{BET} when compared to the reported NiO/CNFs and MgO/ACNF, but the sample has the best CO_2 adsorption capability at 298 K and 1 bar. The 5Ni@CNF material exhibits the lowest S_{BET} when compared to porous CNF without metal oxide dopants. The sample's adsorption performance shows the maximum CO_2 adsorption at both temperatures (273 K and 298 K). However, because of their surface morphologies, 10Ni@CNF and 15Ni@CNF had low CO_2 adsorption amounts at both temperatures. There were Ni/NiO spots all over the surface of the 15Ni@CNF, providing space between the particles and the carbon matrix for the adsorption of CO_2 molecules. Since CO_2 molecules could not be captured by the huge pore size of the 10Ni@CNF surface, despite its high surface porosity, it had the lowest CO_2 uptake capacity.

Table 2. Comparisons of CO_2 uptakes at 1 bar on the adsorbents with various support materials.

Adsorbents	SSA (m^2/g)	Temp.(K)	CO_2 uptake (mmol/g)	Reference
PAN@CNF	306	298	2.52	[74]
Activated-CNF	897	298	3.17	[75]
Hollow ACNF	884	298	3.16	[76]
NiO/CNF	330	298	1.11	[77]
MgO/ACNF	413	298	2.67	[78]
PCNF-2-1000	417	298	3.11	[79]
Porous CNF/C-H	1084	273	5.08	[80]
Porous CNF/C-S	990	273	4.63	[80]
5Ni@CNF	396	273	6.15	This work
5Ni@CNF	396	298	4.28	This work
10Ni@CNF	66	273	0.28	This work
10Ni@CNF	66	298	0.18	This work
1NR-10Ni@CNF	79	273	1.19	This work
1NR-10Ni@CNF	79	298	1.18	This work

The CO_2 adsorption isotherms on nNR-10Ni@CNF samples at different temperatures (273 K and 298 K) are presented in Fig. 15. With increasing amounts of NR content, the amount of CO_2 adsorbed increased. At both temperatures, the adsorption of CO_2 on NR-doped 10Ni@CNF was in the order of 2NR-10Ni@CNF > 1NR-10Ni@CNF > 0.5NR-10Ni@CNF. When loading trace amounts of NR into 10Ni@CNF, the CO_2 uptake capacity increased. This demonstrates that the NR may create small pores in the carbon matrix of these CNF samples and allow CO_2 molecules to adsorb. Compared with those reported in Table 2, the CO_2 adsorption capacity of nNR-10Ni@CNF samples is lower than any porous CNF or metal-doped CNF samples due to the lower surface area and lower porosity. Additionally, all samples gave a CO_2 uptake value higher than 10Ni@CNF. This implies that NR can enhance CO_2 adsorption by generating suitable pores on the CNF surface. Besides, the CNT branches on their CNF surface may contribute to adsorbing CO_2.

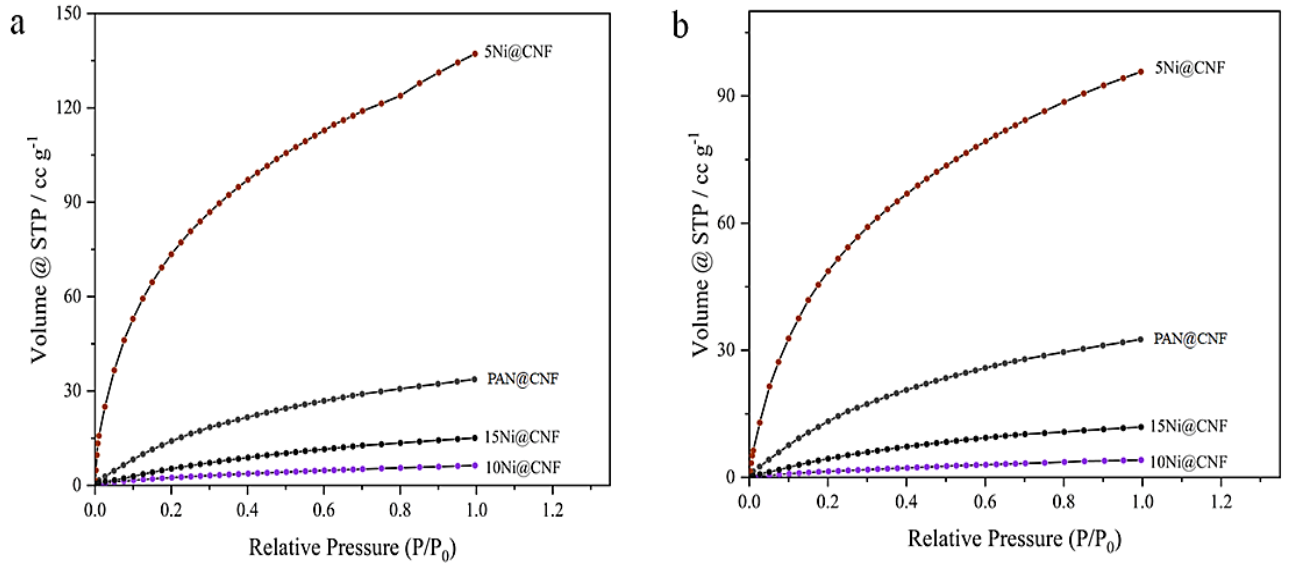

Fig. 14 CO_2 adsorption equilibrium isotherms for nNi@CNF (a) at 273 K and (b) at 298 K.

The 5Ni@CNF sample has the highest CO_2 adsorption capacity (4.28 mmol g^{-1}) when compared to other adsorbent materials, such as metal-organic frameworks (MOFs), zeolite-based materials, and silica-based materials, that have been reported at ambient air (298 K at 1 bar).[81] In contrast to the functionalized MOF materials with the highest CO_2 uptake, the MOFs named 1-en-Mg_2(dobpdc) provides a capacity value of 2.83 mmol g^{-1} less than 5Ni@CNF. The 5Ni@CNF sample nevertheless exhibits greater CO_2 capture performance when compared to adsorbents without surface modification, such as zeolite (Li-LSK) and silica (K_2CO_3/γ-Al_2O_3) materials, which display uptake values of 1.34 and 1.20 mmol g^{-1}, respectively. It is interesting to note that this sample's CO_2 capture capability is comparable to that of ionic liquid (IL) absorbents like Sar (5.4 mmol g^{-1}), GlyGly (3.8 mmol g^{-1}), TBAB (3.8 mmol g^{-1}), and BTIG (3.0 mmol g^{-1}).

4. Conclusions

Diverse Ni@CNF, NR@CNF, and NR-10Ni@CNF samples were successfully prepared by the electrospinning technique, followed by conventional thermal treatment. The Ni^0 form was controlled by incorporating a pyridine ligand. Different Ni nanoparticle sizes influenced pore and spot formation on the CNF surface. NR showed promise as a new carbon additive and natural polymer resource for utilization as a carbon source in the PAN precursor for carbon nanotube fabrication. NR doped in PAN-based CNF increased the diameter of the CNF and produced a smooth surface. Fabricating carbon nanotube

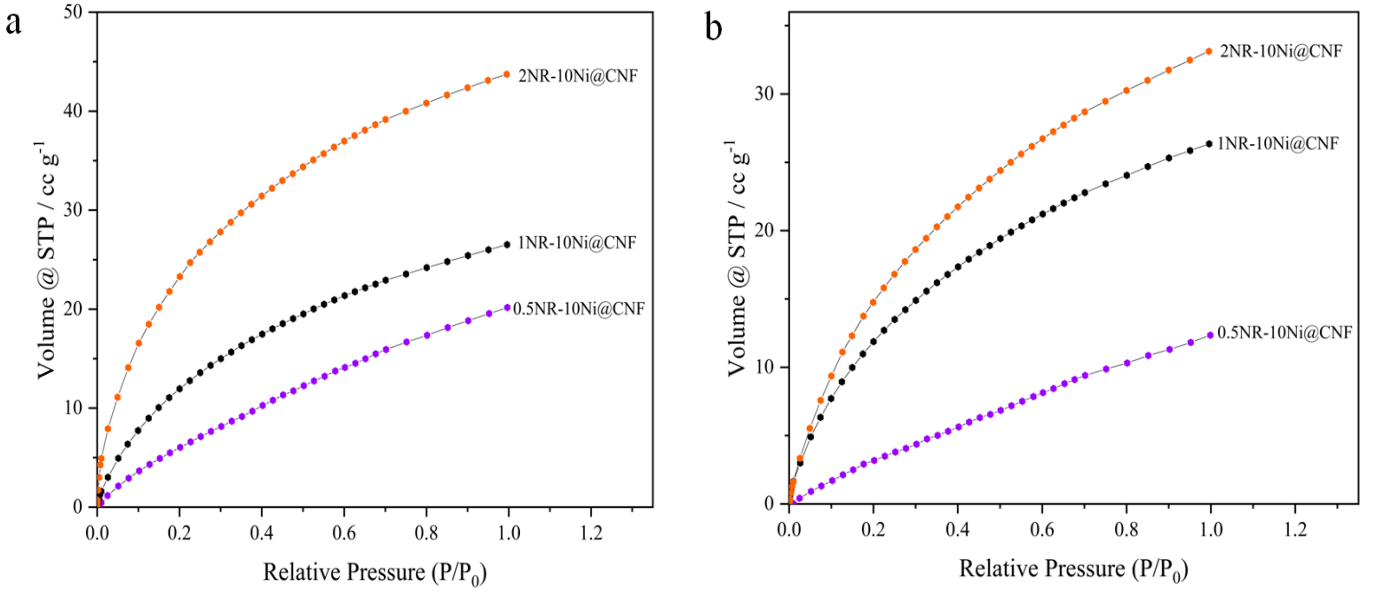

Fig. 15 CO_2 adsorption equilibrium isotherms for nNR-10Ni@CNF (a) at 273 K and (b) at 298 K.

growth on carbon nanofibers was achieved by mixing NR (0.5 to 2 wt%) and Ni (10 wt%), while both metallic Ni nanoparticles and NiO nanoparticles were well dispersed in the carbon nanofiber. Furthermore, small amounts of NR could enhance the specific capacitance (from 40 F/g to 84 F/g) and CO_2 adsorption performance (from 0.28 and 0.18 mmol/g to 1.19 and 1.18 mmol/g at 273 and 298 K, respectively) in 1NR-10Ni@CNF.

Acknowledgements

This work was supported by the Thailand Science Research and Innovation Fundamental Fund fiscal year 2022 (Project No. TUFF07/2565) and Thammasat University Research Fund Contract No. TUFT-FF 22/2565. Research teams are grateful to Prof. Dr. Santi Maensiri, Institute of Science, Suranaree University of Technology for allowing use of his electrospinning machine to prepare electrospun fibers.

Conflict of Interest

There is no conflict of interest.

Supporting Information

Applicable.

References

[1] M. H. Al-Saleh, U. Sundararaj, Review of the mechanical properties of carbon nanofiber/polymer composites, *Composites Part A: Applied Science and Manufacturing*, 2011, **42**, 2126-2142, doi: 10.1016/j.compositesa.2011.08.005.

[2] L.-H. Sun, Z. Ounaies, X.-L. Gao, C. A. Whalen, Z.-G. Yang, Preparation, characterization, and modeling of carbon nanofiber/epoxy nanocomposites, *Journal of Nanomaterials, Preparation,* 2011, 1-8, doi: 10.1155/2011/307589.

[3] J.K. Chinthaginjala, K. Seshan, L. Lefferts, *Industrial & Engineering Chemistry Research*, 2007, **46**, 3968-3978, 10.1021/ie061394r.

[4] B. Ruan, J. Wang, D. Shi, Y. Xu, S. Chou, H. Liu, J. Wang, A phosphorus/N-doped carbon nanofiber composite as an anode material for sodium-ion batteries, *Journal of Materials Chemistry A*, 2015, **3**, 19011-19017, doi: 10.1039/c5ta04366b.

[5] G. Zheng, Y. Yang, J. J. Cha, S. S. Hong, Y. Cui, Hollow carbon nanofiber-encapsulated sulfur cathodes for high specific capacity rechargeable lithium batteries, *Nano Letters*, 2011, **11**, 4462-4467, doi: 10.1021/nl2027684.

[6] H. Kim, S. Lee, Characterization of carbon nanofiber (CNF)/polymer composite coated on cotton fabrics prepared with various circuit patterns, *Fashion and Textiles*, 2018, **5**, 1-13, doi: 10.1186/s40691-017-0120-2.

[7] E. Azwar, W. A. Wan Mahari, J. H. Chuah, D.-V N. Vo, N. L. Ma, W. H. Lam, S. S. Lam, Transformation of biomass into carbon nanofiber for supercapacitor application - A review, *International Journal of Hydrogen Energy*, 2018, **43**, 20811-20821, doi: 10.1016/j.ijhydene.2018.09.111.

[8] X. Shi, W. Zhou, D. Ma, Q. Ma, D. Bridges, Y. Ma, A. Hu, Electrospinning of nanofibers and their applications for energy devices, *Journal of Nanomaterials*, 2015, **16**, 122-122, doi: 10.1155/2015/140716.

[9] M. Sharon, M. Sharon, Carbon Nanofiber: Fundamentals and Applications, Wiley, 2021.

[10] H. Meng, Y. Liu, H. Liu, S. Pei, X. Yuan, H. Li, Y. Zhang, ZIF67@MFC-derived Co/N-C@CNFs interconnected frameworks with graphitic carbon-encapsulated Co nanoparticles as highly stable and efficient electrocatalysts for oxygen reduction reactions, *ACS Applied Materials & Interfaces*, 2020, **12**, 41580-41589, doi: 10.1021/acsami.0c12069.

[11] S. Chanthee, M. Santikunaporn, J. Jirasangthong, C. Asavatesanupap, Synthesis and antimicrobial studies of nano-copper doped carbon substrates; activated carbon, reduced graphene oxide, and carbon nanofiber, *Journal of Magnetism and Magnetic Materials*, 2022, **32**, 68-74, doi: 10.55713/jmmm.v32i3.1270.

[12] S. R. Dhakate, A. Chaudhary, A. Gupta, A. K. Pathak, B. P. Singh, K. M. Subhedar, T. Yokozeki, Excellent mechanical properties of carbon fiber semi-aligned electrospun carbon nanofiber hybrid polymer composites, *RSC Advances*, 2016, **6**, 36715-36722, doi: 10.1039/c6ra02672a.

[13] S. Jiang, Y. Chen, G. Duan, C. Mei, A. Greiner, S. Agarwal, Electrospun nanofiber reinforced composites: a review, *Polymer Chemistry*, 2018, **9**, 2685-2720, doi: 10.1039/c8py00378e.

[14] J.-W. Jung, C.-L. Lee, S. Yu, I.-D. Kim, Electrospun nanofibers as a platform for advanced secondary batteries: a comprehensive review, *Journal of Materials Chemistry A*, 2016, **4**, 703-750, doi: 10.1039/c5ta06844d.

[15] L. Feng, N. Xie, J. Zhong, Carbon nanofibers and their composites: a review of synthesizing, properties and applications, *Materials*, 2014, **7**, 3919-3945, doi: 10.3390/ma7053919.

[16] Z.-M. Huang, Y.-Z. Zhang, M. Kotaki, S. Ramakrishna, A review on polymer nanofibers by electrospinning and their applications in nanocomposites, *Composites Science and Technology*, 2003, **63**, 2223-2253, doi: 10.1016

[17] J. D. Schiffman, C. L. Schauer, A review: electrospinning of biopolymer nanofibers and their applications, *Polymer Reviews*, 2008, **48**, 317-352, doi: 10.1080/15583720802022182.

[18] S. Y. Gu, J. Ren, G. J. Vancso, Process optimization and empirical modeling for electrospun polyacrylonitrile (PAN) nanofiber precursor of carbon nanofibers, *European Polymer Journal*, 2005, **41**, 2559-2568, doi: 10.1016/j.eurpolymj.2005.05.008.

[19] S. Y. Gu, J. Ren, Q. L. Wu, Preparation and structures of electrospun PAN nanofibers as a precursor of carbon nanofibers, *Synthetic Metals*, 2005, **155**, 157-161, doi: 10.1016/j.synthmet.2005.07.340.

[20] Z. Xu, X. Jiang, H. Zhou, J. Li, Preparation of magnetic hydrophobic polyvinyl alcohol (PVA)-cellulose nanofiber (CNF) aerogels as effective oil absorbents, *Cellulose*, 2018, **25**, 1217-1227, doi: 10.1007/s10570-017-1619-9.

[21] P. Wang, D. Zhang, F. Ma, Y. Ou, Q. N. Chen, S. Xie, J. Li, Mesoporous carbon nanofibers with a high surface area

electrospun from thermoplastic polyvinylpyrrolidone, *Nanoscale*, 2012, **4**, 7199, doi: 10.1039/c2nr32249h
[22] B-H. Kim, A. H. Wazir, K. S. Yang, Y. H. Bang, S. R. Kim, Pitch based carbon fibers for automotive body and electrodes, *Carbon Letters*, 2011, **12**, 70-80, doi: 10.5714/CL.2011.12.2.070.
[23] S. H. Park, C. Kim, Y. I. Jeong, D. Y. Lim, Y. E. Lee, K. S. Yang, Activation behaviors of isotropic pitch-based carbon fibers from electrospinning and meltspinning, *Synthetic Metals*, 2004, **146**, 207-212, doi: 10.1016/j.synthmet.2004.07.004.
[24] S. Y. Gu, J. Ren, Q. L. Wu, Preparation and structures of electrospun PAN nanofibers as a precursor of carbon nanofibers, *Synthetic Metals*, 2005, **155**, 157-161, doi: 10.1016/j.synthmet.2005.07.340.
[25] C. D. Workman, S. Hopkins, J. Pant, M. Goudie, H. Handa, Covalently bound *S*-nitroso-*N*-acetylpenicillamine to electrospun polyacrylonitrile nanofibers for multifunctional tissue engineering applications, *ACS Biomaterials Science & Engineering*, 2021, **7**, 5279-5287, doi: 10.1021/acsbiomaterials.1c00907.
[26] S. E. Kim, A. P. Tiwari, Mussel-inspired polydopamine-enabled in situ-synthesized silver nanoparticle-anchored porous polyacrylonitrile nanofibers for wound-healing applications, *International Journal of Polymeric Materials and Polymeric Biomaterials*, 2022, **71**, 471-480, doi: 10.1080/00914037.2020.1857381.
[27] H. Samadian, S. S. Zakariaee, M. Adabi, H. Mobasheri, M. Azami, R. Faridi-Majidi, Effective parameters on conductivity of mineralized carbon nanofibers: an investigation using artificial neural networks, *RSC Advances*, 2016, **6**, 111908-111918, doi: 10.1039/c6ra21596c.
[28] L. Huang, J. Cheng, G. Qu, X. Li, Y. Hu, W. Ni, D. Yuan, Y. Zhang, B. Wang, Porous carbon nanofibers formed *in situ* by electrospinning with a volatile solvent additive into an ice water bath for lithium-sulfur batteries, *RSC Advances*, 2015, **5**, 23749-23757, doi: 10.1039/c4ra14680h.
[29] Y. Chen, X. Li, K.-S. Park, J. Hong, J. Song, L. Zhou, Y.-W. Mai, H. Huang, J. B. Goodenough, Sulfur encapsulated in porous hollow CNTs@CNFs for high-performance lithium-sulfur batteries, *Journal of Materials Chemistry A*, 2014, **2**, 10126-10130, doi: 10.1039/c4ta01823k.
[30] S. H. Yoo, H.-I. Joh, S. Lee, Synthesis of porous carbon nanofiber with bamboo-like carbon nanofiber branches by one-step carbonization process, *Applied Surface Science*, 2017, **402**, 456-462, doi: 10.1016/j.apsusc.2017.01.154.
[31] M. Kumar, M. Hietala, K. Oksman, Lignin-based electrospun carbon nanofibers, *Frontiers in Materials*, 2019, **6**, 62, doi: 10.3389/fmats.2019.00062.
[32] P. B. Santhosh, J. Genova, H. Chamati, Green synthesis of gold nanoparticles: an eco-friendly approach, *Chemistry*, 2022, **4**, 345-369, doi: 10.3390/chemistry4020026.
[33] G. Sui, W. H. Zhong, X. P. Yang, Y. H. Yu, S. H. Zhao, Preparation and properties of natural rubber composites reinforced with pretreated carbon nanotube, *Polymers for Advanced Technologies*, 2008, **19**, 1543-1549, doi: 10.1002/pat.1163.
[34] A. M. Shanmugharaj, J. H.Bae, K. Y. Lee, W. H. Noh, S. H. Lee, S. H. Ryu, Physical and chemical characteristics of multiwalled carbon nanotubes functionalized with aminosilane and its influence on the properties of natural rubber composites, *Composites Science and Technology*, 2007, **67**, 1813-1822, doi: 10.1016/j.compscitech.2006.10.021.
[35] W. Dang, J. Liu, X. Wang, K. Yan, A. Zhang, J. Yang, L. Chen, J. Liang, Structural transformation of polyacrylonitrile (PAN) fibers during rapid thermal pretreatment in nitrogen atmosphere, *Polymers*, 2020, **12**, 63, doi: 10.3390/polym12010063.
[36] M. C. Neary, G. Parkin, Structural characterization of the nickel(II) formate complex, $Ni(py)_4(O_2CH)_2{\cdot}2py$, and re-evaluation of the nitrate counterpart, $Ni(py)_4(ONO_2)_2{\cdot}2py$: evidence for non-linear nitrate coordination, *Polyhedron*, 2016, **116**, 189-196, doi: 10.1016/j.poly.2016.04.033.
[37] A. L. Patterson, The scherrer formula for X-ray particle size determination, *Physical Review*, 1939, **56**, 978-982, doi: 10.1103/physrev.56.978.
[38] P. Khamnantha, C. Homla-or, K. Suttisintong, J. Manyam, M. Raita, V. Champreda, V. Intasanta, H.-J. Butt, R. Berger, A. Pangon, Stable lignin-rich nanofibers for binder-free carbon electrodes in supercapacitors, *ACS Applied Nano Materials*, 2021, **4**, 13099-13111, doi: 10.1021/acsanm.1c02637.
[39] M. Yu, C. Wang, Y. Bai, Y. Wang, Q. Wang, H. Liu, Combined effect of processing parameters on thermal stabilization of PAN fibers, *Polymer Bulletin*, 2006, **57**, 525-533, doi: 10.1007/s00289-006-0581-8.
[40] S. Arbab, A. Zeinolebadi, A procedure for precise determination of thermal stabilization reactions in carbon fiber precursors, *Polymer Degradation and Stability*, 2013, **98**, 2537-2545, doi: 10.1016/j.polymdegradstab.2013.09.014.
[41] C. W. Frank, L. B. Rogers, Infrared spectral study of metal-pyridine, -substituted pyridine, and-quinoline complexes in the 667-150 Cm^{-1} region, *Inorganic Chemistry*, 1966, **5**, 615-622, doi: 10.1021/ic50038a026.
[42] S. Akyüz, J. Incl. Phenom., An infrared and raman spectroscopic study of metal(II) Di(2-methylpyridine) tetracyanonickelate complexes: $Ni(C_6H_7N)_2Ni(CN)_4$ and $Cd(C_6H7N)_2Ni(CN)_4$, 1985, **3**, 403–407, doi: 10.1007/BF00657492.
[43] J. S. Im, J. G. Kim, Y.-S. Lee, Fluorination effects of carbon black additives for electrical properties and EMI shielding efficiency by improved dispersion and adhesion, *Carbon*, 2009, **47**, 2640-2647, doi: 10.1016/j.carbon.2009.05.017.
[44] Y. Huang, N. Li, Y. Ma, F. Du, F. Li, X. He, X. Lin, H. Gao, Y. Chen, The influence of single-walled carbon nanotube structure on the electromagnetic interference shielding efficiency of its epoxy composites, *Carbon*, 2007, **45**, 1614-1621, doi: 10.1016/j.carbon.2007.04.016.
[45] R. Andrews, D. Jacques, D. Qian, E. C. Dickey, Purification and structural annealing of multiwalled carbon nanotubes at graphitization temperatures, *Carbon*, 2001, **39**, 1681-1687, doi: 10.1016/s0008-6223(00)00301-8.

[46] A. M. Al-Enizi, M. A. Ghanem, A. A. El-Zatahry, S. S. Al-Deyab, Nickel oxide/nitrogen doped carbon nanofibers catalyst for methanol oxidation in alkaline media, *Electrochimica Acta*, 2014, **137**, 774-780, doi: 10.1016/j.electacta.2014.05.150.
[47] M. R. Rosenthal, R. S. Drago, Pyridine complexes of nickel(II), *Inorganic Chemistry*, 1965, **4**, 840-844, doi: 10.1021/ic50028a015.
[48] D.V. Soldatov, J. Lipkowski, E.V. Grachev Crystal structure of the dinitratotetrakis(pyridine)nickel(II) clathrate with pyridine as guest, $[NiPy_4(NO_3)_2]\cdot{}_2Py$, *Journal of Structural* Chemistry, 1995, **36**, 830-836, doi: 10.1007/bf02579677.
[49] H. Zhang, L. Fang, Dichloro-tetrapyridine-nickel(II) 0.76-hydrate, *Acta Crystallographica Section E: Crystallographic Communications*, 2005, **61**, 180-182, doi: 10.1107/S1600536804033586.
[50] R.V. Biagetti, H.M. Haendler, Pyridine Complexes of Cobalt(II) and Nickel(II) Nitrates, *Inorganic Chemistry*, 1966, **5**, 383-386, doi: 10.1021/ic50037a012.
[51] O. D. I. Prasiwi, T. E. Saraswati, M. Anwar, A. Masykur, Magnetic carbon nanofibers prepared with ni and ni/graphitic carbon nanoparticle catalysts for glycine detection using surface-enhanced raman spectroscopy, *ACS Applied Nano Materials*, 2021, **4**, 6594-6608, doi: 10.1021/acsanm.1c00111.
[52] C-S. Yang, Z. Sun, C-H. Cui, C. Yang, T. Zhang, Metal nano-drills directionally regulate pore structure in carbon, *Carbon*, 2021, **175**, 60-68, doi: 10.1016/j.carbon.2020.12.065.
[53] L. Ci, Z. Xu, L. Wang, W. Gao, F. Ding, K.F. Kelly, B. I. Yakobson, P. M. Ajayan, Controlled nanocutting of graphene, *Nano Research*, 2008, **1**, 116-122, doi: 10.1007/s12274-008-8020-9.
[54] N. Severin, S. Kirstein, I. M. Sokolov, J. P. Rabe, Rapid trench channeling of graphenes with catalytic silver nanoparticles, *Nano Letters*, 2009, **9**, 457-461, doi: 10.1021/nl8034509.
[55] A. M. Al-Enizi, A. A. Elzatahry, A. M. Abdullah, M. A. AlMaadeed, J. Wang, D. Zhao, S. Al-Deyab, Synthesis and electrochemical properties of nickel oxide/carbon nanofiber composites, *Carbon*, 2014, **71**, 276-283, doi: 10.1016/j.carbon.2014.01.052.
[56] N. M. Rodriguez, A review of catalytically grown carbon nanofibers, *Journal of Materials Research*, 1993, **8**, 3233-3250, doi: 10.1557/jmr.1993.3233.
[57] K. P. De Jong, J. W. Geus, Carbon nanofibers: catalytic synthesis and applications, *Catalysis Reviews*, 2000, **42**, 481-510, doi: 10.1081/cr-100101954.
[58] S. Smart, S. Liu, J. M. Serra, J. C. Diniz da Costa, A. Iulianelli, A. Basile, Porous ceramic membranes for membrane reactors. Handbook of Membrane Reactors. Amsterdam: Elsevier, 2013: 298-336, doi: 10.1533/9780857097330.2.298.
[59] J. Choma, M. Kloske, M. Jaroniec, An improved methodology for adsorption characterization of unmodified and modified silica gels, *Journal of Colloid and Interface Science*, 2003, **266**, 168-174, doi: 10.1016/s0021-9797(03)00573-3.
[60] W. Zhelin, J. Xuewei, P. Mao, S. Yongmin, Nano-scale pore structure and its multi-fractal characteristics of tight sandstone by N_2 adsorption/desorption analyses: a case study of shihezi formation from the sulige gas filed, ordos basin, china, *Minerals*, 2020, **10**, 377-398, doi: 10.3390/min10040377.
[61] Y. Poonam, M. Wahid, K.D. Pravin, A.J. Lathe, V.S. Manjusha, Electrospun nanofibers of tin phosphide $SnP_{0.94}$) nanoparticles encapsulated in a carbon matrix: a tunable conversion-cum-alloying lithium storage anode, *Energy Fuels*, 2020, **34**, 7648-7657, doi: 10.1021/acs.energyfuels.0c01046.
[62] T. S. Mathis, N. Kurra, X. Wang, D. Pinto, P. Simon, Y. Gogotsi, Energy storage data reporting in perspective—guidelines for interpreting the performance of electrochemical energy storage systems, *Advanced Energy Materials*, 2019, **9**, 1902007, doi: 10.1002/aenm.201902007.
[63] V. Augustyn, P. Simon, B. Dunn, Pseudocapacitive oxide materials for high-rate electrochemical energy storage, *Energy & Environmental Science*, 2014, **7**, 1597, doi: 10.1039/c3ee44164d.
[64] M. Huang, Y. Lin, H. Huang, X. Fan, K. Shi, Z. Yang, W. Zhang, Nickel nanoparticles modified MnO nanosheet arrays for high-performance supercapacitor with long-lasting and sustainable capacitance increase, *Electrochimica Acta*, 2021, **383**, 138353, doi: 10.1016/j.electacta.2021.138353.
[65] K. Zhang, J. Sun, Lei E, C. Ma, S. Luo, Z. Wu, W. Li, S. Liu, Effects of the Pore Structure of Commercial Activated Carbon on the Electrochemical Performance of Supercapacitors, *Journal of Energy Storage*, 2022, **45**, 103457, doi: 10.1016/j.est.2021.103457.
[66] C. Largeot, C. Portet, J. Chmiola, P.-L. Taberna, Y. Gogotsi, P. Simon, Relation between the ion size and pore size for an electric double-layer capacitor, *Journal of the American Chemical Society*, 2008, **130**, 2730-2731, doi: 10.1021/ja7106178.
[67] A.P. Tiwari, T. Mukhiya, A. Muthurasu, K. Chhetri, M. Lee, B. Dahal, P.C. Lohani, H-Y. Kim, A Review of Electrospun Carbon Nanofiber-Based Negative Electrode Materials for Supercapacitors, *Electrochem,* 2021, **2**, 236-250, doi: 10.3390/electrochem2020017.
[68] X-Y. Li1, Y. Yan, B. Zhang, T-J. Bai, Z-Z. Wang, T-S. He, PAN-derived electrospun nanofibers for supercapacitor applications: ongoing approaches and challenges, *Journal of Materials Science*, 2021, **56**, 10745-10781, doi: 10.1007/s10853-021-05939-6.
[69] Y-C. Chiang, W-L. Hsu, S-Y. Lin, R-S. Juang, Enhanced CO_2 adsorption on activated carbon fibers grafted with nitrogen-doped carbon nanotubes, *Materials*, 2017, **10**, 511-523, doi: 10.3390/ma10050511.
[70] S.-M. Hong, S. H. Kim, B. G. Jeong, S. M. Jo, K. B. Lee, Development of porous carbon nanofibers from electrospun polyvinylidene fluoride for CO_2 capture, *RSC Advances*, 2014, **4**, 58956-58963, doi: 10.1039/c4ra11290c.
[71] F. E. C. Othman, N. Yusof, S. Samitsu, N. Abdullah, M. F. Hamid, K. Nagai, M. N. Z. Abidin, M. A. Azali, A. F. Ismail, J. Jaafar, F. Aziz, W. N. W. Salleh, Activated carbon nanofibers incorporated metal oxides for CO_2 adsorption: effects of different type of metal oxides, *Journal of CO_2 Utilization*, 2021, **45**, 101434, doi: 10.1016/j.jcou.2021.101434.

[72] Y. Li, B. Zou, C. Hu, M. Cao, Nitrogen-doped porous carbon nanofiber webs for efficient CO_2 capture and conversion, *Carbon*, 2016, **99**, 79-89, doi: 10.1016/j.carbon.2015.11.074.
[73] F. E. Che Othman, N. Yusof, J. González-Benito, X. Fan, A. F. Ismail, Electrospun composites made of reduced graphene oxide and polyacrylonitrile-based activated carbon nanofibers (rGO/ACNF) for enhanced CO_2 adsorption, *Polymers*, 2020, **12**, 2117, doi: 10.3390/polym12092117.
[74] Y.-C. Chiang, S.-T. Lee, Y.-J. Leo, T.-L. Tseng, Importance of pore structure and surface chemistry in carbon dioxide adsorption on electrospun carbon nanofibers, *Sensors and Materials*, 2020, **32**, 2277, doi: 10.18494/sam.2020.2871.
[75] Y. C. Chiang, C. Y. Wu, Y. J. Chen, Effects of activation on the properties of electrospun carbon nanofibers and their adsorption performance for carbon dioxide, *Separation and Purification Technology*, 2020, **233**, 116040, doi: 10.1016/j.seppur.2019.116040.
[76] Y.-C. Chiang, C.-C. Huang, W.-T. Chin, Carbon dioxide adsorption on carbon nanofibers with different porous structures, *Applied Sciences*, 2021, **11**, 7724, doi: 10.3390/app11167724.
[77] Q. Li, J. Guo, D. Xu, J. Guo, X. Ou, Y. Hu, H. Qi, F. Yan, Electrospun N-doped porous carbon nanofibers incorporated with NiO nanoparticles as free-standing film electrodes for high-performance supercapacitors and CO_2 capture, *Small*, 2018, **14**, 141704203, doi: 10.1002/smll.201704203.
[78] F. E. C. Othman, N. Yusof, S. Samitsu, N. Abdullah, M. F. Hamid, K. Nagai, M. N. Z. Abidin, M. A. Azali, A. F. Ismail, J. Jaafar, F. Aziz, W. N. W. Salleh, Activated carbon nanofibers incorporated metal oxides for CO_2 adsorption: effects of different type of metal oxides, *Journal of CO_2 Utilization*, 2021, **45**, 101434, doi: 10.1016/j.jcou.2021.101434.
[79] G. Zainab, A. A. Babar, N. Ali, A. A. Aboalhassan, X. Wang, J. Yu, B. Ding, Electrospun carbon nanofibers with multi-aperture/opening porous hierarchical structure for efficient CO_2 adsorption, *Journal of Colloid and Interface Science*, 2020, **561**, 659-667, doi: 10.1016/j.jcis.2019.11.041.
[80] S. Ma, Y. Wang, Z. Liu, M. Huang, H. Yang, Z.-L. Xu, Preparation of carbon nanofiber with multilevel gradient porous structure for supercapacitor and CO_2 adsorption, *Chemical Engineering Science*, 2019, **205**, 181-189, doi: 10.1016/j.ces.2019.05.001.